Weather and Climate Extremes 42 (2023) 100627

Contents lists available at ScienceDirect

Weather and Climate Extremes

journal homepage: www.elsevier.com/locate/wace

Stratosphere-troposphere coupling during stratospheric extremes in the 2022/23 winter

Qian Lu [a,c], Jian Rao [a,*], Chunhua Shi [a], Rongcai Ren [b,a], Yimin Liu [b], Siming Liu [d]

[a] Key Laboratory of Meteorological Disaster, Ministry of Education (KLME), Joint International Research Laboratory of Climate and Environment Change (ILCEC), Collaborative Innovation Center on Forecast and Evaluation of Meteorological Disasters (CIC-FEMD), Nanjing University of Information Science and Technology, Nanjing, 210044, China

[b] National Key Laboratory of Atmospheric Sciences and Geophysical Fluid Dynamics (LASG), Institute of Atmospheric Physics, Chinese Academy of Sciences, Beijing, 100029, China

[c] China Meteorological Administration Xiong-An Atmospheric Boundary Layer Laboratory, Xiong-An, 071800, China

[d] Department of the Geophysical Sciences, University of Chicago, Chicago, 60637, USA

ARTICLE INFO

Keywords:
Sudden stratospheric warming (SSW)
Stratospheric disturbance
Stratospheric water vapor
Ozone

ABSTRACT

Using the ERA5 reanalysis, sea surface temperature, sea ice observations, and the real-time multivariate Madden-Julian Oscillation (MJO) index, the evolution of the stratospheric extreme circulation in the winter of 2022/2023 is explored. The stratospheric polar vortex was disturbed three times in the 2022/23 winter, contrasted with only one disturbance during the other three recent winters with an SSW. Possible favorable conditions for the strong stratospheric disturbances and their effects on stratospheric ozone, water vapor distribution, and near-surface temperature were examined. Around 7 December 2022 when a short but strong pulse of planetary wavenumber 2 appeared from the troposphere to stratosphere, a weakened and elongated stratospheric polar vortex formed at 10 hPa. This pulse is related to the intensifying Ural ridge and the deepening East Asian trough. After the first stratospheric disturbance, a large fraction of cold anomalies occurred in the Eurasian continent. A lagged impact after these stratospheric disturbances was observed as strong cold anomalies formed in North America from 13 to 23 December. On 28 January 2023, a minor SSW event occurred due to a displacement of the stratospheric polar vortex. A strong pulse of eddy heat flux contributed alternately by planetary wavenumber 1 and 2 showed a large accumulative effect on the stratospheric disturbance. However, the downward impact of this second disturbance was weak, and cold surges were not noticeable after this minor SSW. The third stratospheric disturbance this winter is a major displace-type SSW that occurred on 16 February 2023, and the total eddy heat flux primarily contributed by planetary wavenumber 1 increased rapidly. Following the major SSW, the North American continent was covered by large patches of strong cold anomalies until the end of March. During the three disturbances, the residual circulation correspondingly strengthened. The water vapor and ozone in the middle and lower layers of the polar stratosphere showed positive anomaly disturbances, especially after the major SSW onset. The unprecedented frequent stratospheric disturbances in winter 2022/23 were accompanied by severe loss of Barents-Laptev Sea ice and anomalously cold tropical Pacific sea surface temperatures (La Niña), which have been reported to be conducive to the enhancement of planetary waves 1 and 2 respectively. Further, two weeks before the major SSW, existing MJO developed into phases 4–6, also contributing to the occurrence of major SSW.

1. Introduction

The stratospheric polar vortex (SPV) is a large-scale circulation system that occupies the polar region in winter and plays an important role in the stratosphere-troposphere coupling (Matsuno, 1971; Held et al., 2002; Tian et al., 2023). The stratospheric polar vortex state is an important source for improving the predictability of the troposphere in subseasonal to seasonal (S2S) time scales (Tripathi et al., 2015; Rao et al., 2019b, 2022, 2023; Domeisen and Butler, 2020; Domeisen et al., 2020a; 2020b). Recent studies have linked the stretching of the SPV to

* Corresponding author. Student Activity Center, Room 308, Ningliu Road # 219, Pukou District, Nanjing, Jiangsu, China.
E-mail address: raojian@nuist.edu.cn (J. Rao).

https://doi.org/10.1016/j.wace.2023.100627
Received 9 July 2023; Received in revised form 2 November 2023; Accepted 9 November 2023
Available online 13 November 2023

the extreme coldness in parts of Eurasia and North America (Cohen et al., 2021; Ding et al., 2023). The strength and position of the stratospheric polar vortex are affected by the planetary-scale Rossby waves, which propagate vertically from the troposphere to the polar stratosphere and break up there (Charney and Drazin, 1961; Polvani and Waugh, 2004; Zhang et al., 2016). In some winters with strong influence of breaking planetary waves that propagate from the troposphere to the stratosphere, the stratospheric westerly winds in the circumpolar regions reverse to easterlies, and the temperature gradient from mid-to-high latitudes reverses, which is termed major sudden stratospheric warming (SSW) event in existing literature (Butler et al., 2015; Rao et al., 2019a; Baldwin et al., 2021). In some winters, a minor SSW event occurs when the temperature in the stratospheric polar cap increases and the temperature gradient reverses, while circumpolar westerly winds decelerate but do not reverse to easterlies (Limpasuvan et al., 2004; Baldwin et al., 2021).

SSW occurs much more frequently in the Arctic than in the Antarctic, and it occurs approximately six to seven times per decade in the Northern Hemisphere (NH) (Charlton and Polvani, 2007; Cao et al., 2019; Rao et al., 2021). However, in the Southern Hemisphere (SH) only one major SSW was observed in September 2002 (Allen et al., 2006; Liu and Roble, 2005), although a similar phenomenon occurred in early September 2019, which was a minor SSW (Rao et al., 2020b; Shen et al., 2020). According to the shape and structure of the stratospheric polar vortex, major SSW events are classified as vortex displacement and split types (Charlton and Polvani, 2007; Seviour et al., 2013). The vortex displacement SSW is featured with the polar vortex deviating from the polar region, and the vortex split SSW is characterized by the elongation and splitting of the polar vortex (Rao and Garfinkel, 2020a; Baldwin et al., 2021). Some SSWs are associated with an enhancement of the planetary waves from the troposphere (Yoden et al., 1999). Planetary wave sources near the tropopause may also play an important role in the development of SSWs (de la Cámara et al., 2019; Boljka and Birner, 2020).

During the occurrence of the SSWs, the stratospheric circulation anomalies resemble a circular dipole mode, known as the northern annular mode (NAM) (Baldwin and Dunkerton, 2001; Baldwin and Thompson, 2009). With the downward propagation of the NAM signal associated with the stratospheric disturbance, the tropospheric Arctic Oscillation (AO) develops toward its negative phase (Karpechko et al., 2018), and the chance of continental-scale cold air outbreaks increases (Thompson et al., 2002; Yu et al., 2015; Lu et al., 2021b). It has been found that SSW can also affect the sub-seasonal variability of the air quality near the surface and modulate the diffusion conditions of atmospheric particles (Lu et al., 2021a, 2022a, 2022b; Dai et al., 2022).

Both observations and modeling studies suggest that differences may exist between the effects of displacement and split SSWs on the troposphere and near-surface. The statistics from the limited observation samples show that the split SSWs have a longer duration and a stronger downward propagation. As a consequence, the effect of split SSWs on the near-surface is greater and more evident than those of displacement SSWs (Rao and Garfinkel, 2020a; Liang et al., 2022; Lu et al., 2022a). However, this difference is not present as the sample size increases using model simulations (Maycock and Hitchcock, 2015; White et al., 2019). In addition, SSW events also affect the distribution of stratospheric gases such as ozone and water vapor (Schoeberl and Hartmann, 1991; Manney et al., 2009; de la Cámara et al., 2018a, 2018b).

Key factors that influence the stratospheric polar vortex include the quasi-biennial oscillation (QBO), El Niño–Southern Oscillation (ENSO), and Arctic sea ice (Baldwin et al., 2021). It is widely reported that the stratospheric polar vortex tends to be colder and stronger during the westerly QBO phase, while it is anomalously warm and weak during the QBO easterly phase (Andrews et al., 2019; Anstey and Shepherd, 2014; Chen and Wei, 2009). Statistics from observations have shown that the SSWs appear more frequently during the easterly QBO than during the westerly QBO phase (Rao et al., 2019a). Similarly, the reduction of Arctic sea ice and moderate El Niños are conducive to the enhancement of planetary waves from the troposphere to the stratosphere and the onset of SSW events (Kim et al., 2014; Lu et al., 2021b; Rao et al., 2020a).

During the period 2014–2023, four major SSWs have occurred in the Northern Hemisphere. However, the stratospheric polar vortex in the 2022/23 winter was very different from the other SSWs (February 2018, January 2019, and January 2021). The stratospheric polar vortex was disturbed three times in the 2022/23 winter, contrasted with only one disturbance during the other three recent winters with an SSW (Fig. 1). As the two disturbances (December 2022, January 2023) in early-to-midwinter of 2022/23 failed to excite a sudden warming event, the weak vortex persisted until February 2023. Another tropospheric wave pulse appeared in February 2023 and finally led to the onset of a major SSW. This study aims to examine the evolution of the stratospheric circulation during this particular winter, which has not been reported.

The paper is organized as follows. Following the introduction, section 2 presents the data and methodology. Section 3 displays the evolution of the stratospheric polar vortex in the winter of 2022/23. Section 4 shows the effects of SSWs on near-surface 2m temperature, stratospheric water vapor, and ozone. Section 5 explores the background conditions, which are possibly conducive to the 2022/23 SSW. Finally, section 6 gives the conclusion and discussion.

2. Data and methodology

2.1. Data

This study uses the fifth-generation reanalysis (ERA5) data from the European Centre for Medium Range Weather Forecasts (ECMWF) from

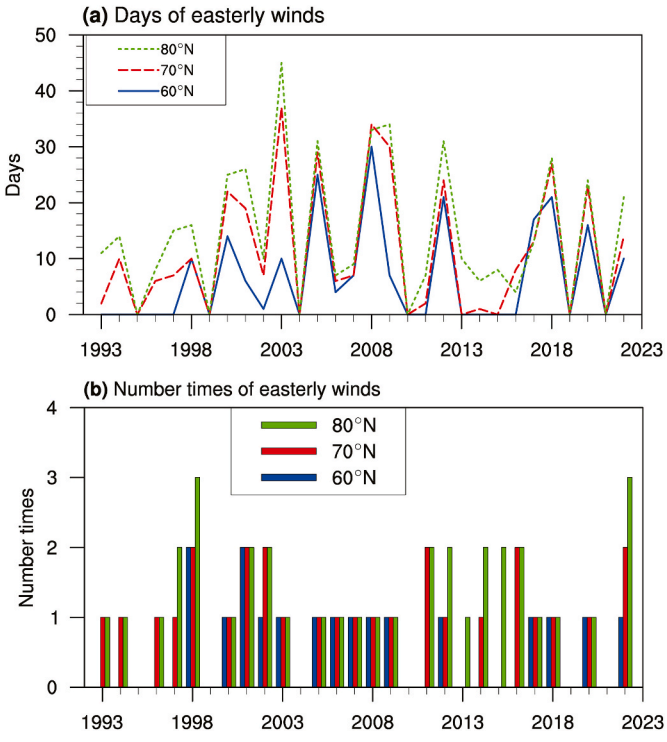

Fig. 1. Statistics of Arctic polar vortex disturbances in winter (December to February) from 1993/94 to 2022/23. (a) Days with easterly winds at three latitudes (60°N, 70°N, and 80°N) on 10 hPa. (b) The number of times the zonal mean zonal wind reversals from lasting westerlies to easterlies at three latitudes (60°N, 70°N, and 80°N) on 10 hPa. Time interval between the end of the first easterly wind disturbance and the beginning of the following easterly disturbances in the same winter is greater than 15 days. The year 1993 shows the winter of 1993/94.

1950 to 2023. The ERA5 reanalysis has a nominal 0.25° × 0.25° resolution with the model top at 0.01 hPa. For easy handling, the data was collected at a horizontal resolution of 1° (latitude) × 1° (longitude) at 37 pressure levels from 1 000 to 1 hPa in the vertical direction (Hersbach et al., 2020). The variables of ERA5 reanalysis at pressure levels analyzed in this study include geopotential height, zonal and meridional winds, air temperature, water vapor, and ozone. One-single-level variables used in this study include 2-m temperature.

Monthly sea ice concentration and sea surface temperature data during 1950–2023 were provided by the Met Office Hadley Centre (HadISST1), with a horizontal resolution of 1° × 1°(Rayner et al., 2003). The real-time multivariate Madden Julian Oscillation (MJO) index was used to test the possible impact of the tropical intraseasonal oscillation on the occurrence of SSWs (Wheeler and Hendon, 2004).

2.2. Methods

The climatology of each variable is calculated using the long-term average from 1979 to 2022. The anomalies for a variable refer to deviations between the raw daily data and the smoothed (31-day running mean) daily climatology.

Since the vertical component (Fz) of the Eliassen-Palm (E-P) flux is approximately proportional to the transient eddy heat flux, daily meridional wind and temperature are used to calculate the eddy heat flux ($\overline{v^*T^*}$) in this study, where the overbar indicates the zonal average and the asterisk indicates the zonal deviation. The eddy heat flux area-weighted average from 45 to 75°N at 300 hPa and 100 hPa is used to represent the vertical propagation of planetary waves from the troposphere and lower stratosphere (de la Cámara et al., 2019; Polvani and Waugh, 2004). Since only planetary waves can propagate upward into the stratosphere (Nishii et al., 2009), the eddy heat flux components by the planetary waves 1–3 are diagnosed.

The stratospheric column ozone (STO3) is computed by vertically integrating the ozone mixing ratio (RO3) divided by the gravitational acceleration: $STO3 = \frac{1}{g}\iint_{Pt}^{Ps} RO3dP$, where Pt is the tropopause pressure, taken as 200 hPa, Ps is the stratopause pressure, taken as 1 hPa, and g is the gravitational acceleration constant (g = 9.8 m/s^2). The unit of the STO3 is converted from kg/m^2 to Dobson unit (DU) with a rough estimate of 1 DU = 2.1415 × 10^{-5} kg/m^2 (Rao and Garfinkel, 2020b).

When calculating Brewer Dobson circulation (BDC), the vertical residual velocity is computed as follows: $\overline{\omega}^* = \overline{\omega} - \frac{\partial}{r_0 \cos\varphi \partial\varphi}\left(\frac{\overline{v\theta}\cos\varphi}{\overline{\theta}_P}\right)$, ω is the vertical wind component, $\boldsymbol{\theta}$ is potential temperature, r_0 is the Earth's radius, φ is latitude, and P is the pressure. The overbars denote zonal average, and the prime denotes the zonal deviation, the subscript P represents the derivative of pressure (Andrews et al., 1987).

3. Evolution of the stratospheric polar vortex during the winter of 2022/23

3.1. Overview of Arctic polar vortex disturbances in recent 30 years

Fig. 1 shows the statistics of the stratospheric disturbances by examining the evolution of the number of days of zonal-mean easterlies at three latitudes (60°N, 70°N, 80°N) at 10 hPa in the past three decades. In general, the zonal mean zonal wind disturbance is more frequent around the pole, which might be due to the distant position from the westerly jet core. Both the number of easterly days in winter and the times of the zonal mean zonal wind reversals from westerlies to easterlies are the highest in the 80°N latitude near the polar region than for the other two latitudes (Butler and Gerber, 2018). In the winter of 2003/04, there were the most easterly days at 80°N and 70°N, but the stratospheric disturbance occurred only once at each of the three latitudes. In the winter of 2008/09, the number of easterly days at 60°N was the largest, which was related to the SSW occurring on January 24 and its long duration, but the stratospheric disturbance occurred only once. It is worth noting that three stratospheric disturbances occurred in the winter of 2022/23 at 80°N, which is very rare in the past three decades except in the winter of 1998/99. In the last decade, such frequent stratospheric disturbances only formed once. Although two disturbances were also observed in three winters (2014/15, 2015/16, and 2016/17), no major SSW formed in those winters.

3.2. Minor and major SSWs in 2022/23 winter

The time evolution of several atmospheric parameters from 16 November 2022 to 1 April 2023 is shown in Fig. 2. During December 6–8, 2022, the westerly winds at 70°N and 80°N decelerated rapidly, and the zonal winds at latitude 80°N even reversed to easterlies (Fig. 2a). However, the observed temperature gradient between 80°N and 60°N showed no reversal in its sign (Fig. 2d). Therefore, the first disturbance of the stratospheric polar vortex was short-lived and weak. On 28 January 2023, another rapid decline in westerly winds was observed, with westerly winds at 60°N dropping to below 15 m/s; the westerly winds at 70°N and 80°N even reversed to easterly winds with the maximum easterly winds of >18 m/s at 80°N for 6 days (Fig. 2a). At the same time, the reversal of temperature gradient between 60°N and the North Pole was observed, with the maximum temperature difference between 80°N and 60°N around 12 K (Fig. 2d). Therefore, the second disturbance of the stratosphere was a minor SSW. Since 16 February 2023, the westerly winds at 60°N changed to the easterly winds and lasted for 23 days with intermittent westerly recoveries for 2 days. Further, the temperature gradient in the polar cap was also reversed, and the maximum temperature difference between 80°N and 60°N reached >29 K. Therefore, the third disturbance of the stratosphere in the 2022/23 winter was a major SSW. The duration of the major SSW (16 February) was very long, three times the average duration of historical SSWs (8 days) (Rao et al., 2021). This mainly reflects a persistent strong dynamic forcing that overwhelms the non-adiabatic cooling effect during this period.

The latitude-time evolution of zonal wind anomalies at 10 hPa was also examined (Fig. 2b). For the first disturbance on 7 December 2022, the local easterly anomalies extended southward from the polar region to ~65°N with the maximum amplitude around 20 m/s between 75°N and 85°N. For the minor SSW on 28 January 2023, the easterly anomalies expanded southward to 60°N with the maximum amplitude around 30 m/s near 75°N. The gradual poleward propagation of the easterly anomalies from midlatitudes to the North Pole was evident in January 2023. When the major SSW occurred, the easterlies reached the North Pole, and the wind anomalies gradually amplified.

Based on the height-time evolution of the zonal wind anomalies at 70°N (Fig. 2c), the first rapid disturbance showed simultaneous easterly wind anomalies from the stratosphere to the near surface. The easterly wind anomalies during the minor SSW only propagate downward to 50 hPa. The easterly wind anomalies during the major SSW lasted from mid-February to end of March, with the wind anomalies propagating downward to 200 hPa.

From the latitude-time evolution of the temperature anomalies at 10 hPa (Fig. 2e), the first stratospheric disturbance around 7 December 2022 was not accompanied by warm anomalies, and cold anomalies (~-10K) developed poleward of 60°N. In contrast, the warm anomalies are more evident during the minor and major SSWs. The warm anomalies during the minor SSW around 28 January can extend southward of 50°N. The maximum warm anomalies formed in the polar region following the onset of the major SSW (20–30 K). The poleward propagation of easterly anomalies was also accompanied by the poleward propagation of the warm anomalies from midlatitudes to the Arctic (Fig. 2e vs Fig. 2b).

The pressure-time evolution of temperature anomalies further confirms that cold stratospheric anomalies dominated in early winter while the warm stratospheric anomalies prevailed in late winter (Fig. 2f). A

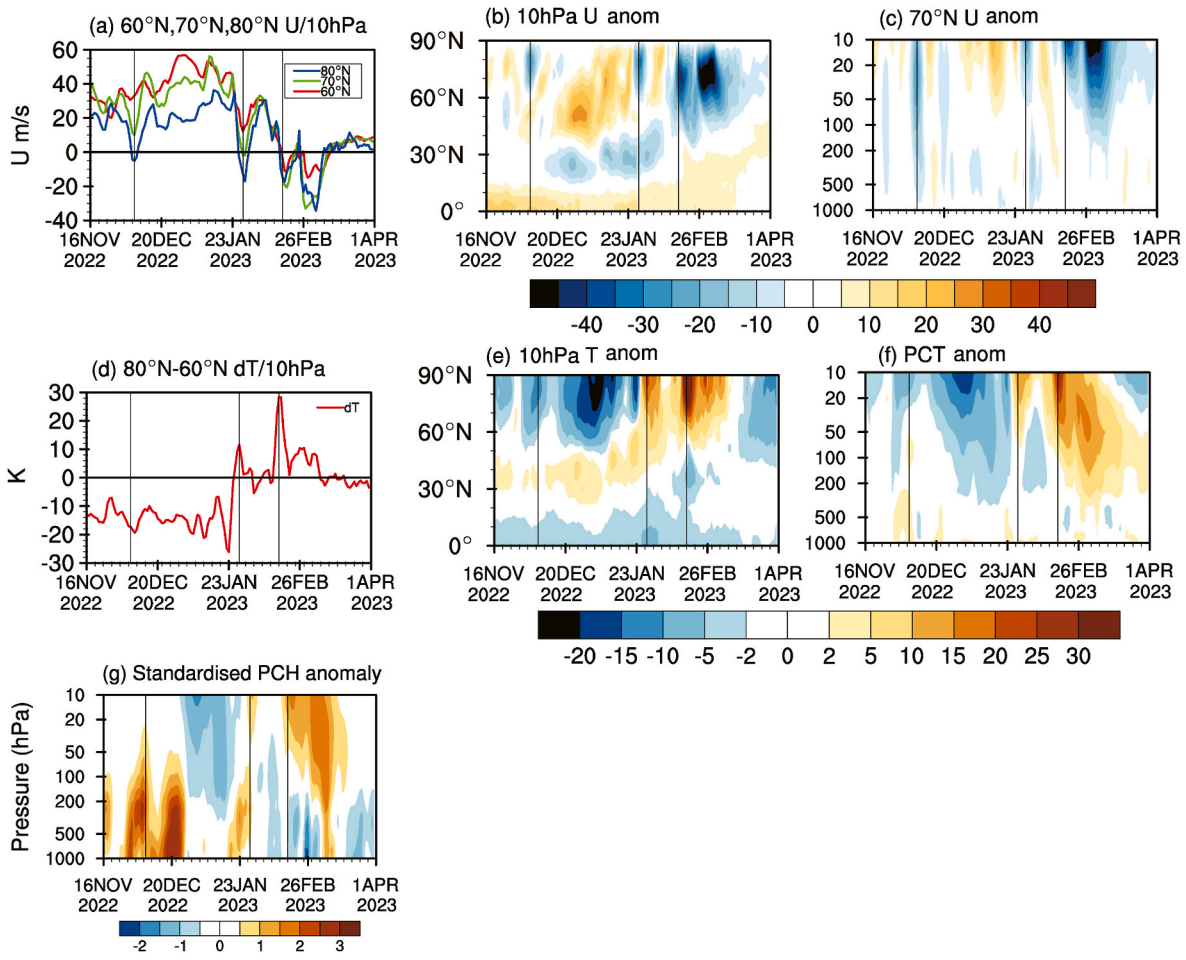

Fig. 2. Time evolution of several metrics from 16 November 2022 to 1 April 2023. (a) Zonal mean zonal wind anomalies at three latitudes (60°N, 70°N, and 80°N) on 10 hPa (unit: m/s). (b) Latitude-time evolution of zonal mean zonal wind anomalies at 10 hPa (shadings, unit: m/s). (c) Pressure-time evolution of zonal mean zonal wind anomalies at 70°N (shadings, unit: m/s). (d) Evolution of the temperature gradient in the polar cap region denoted by the temperature difference between 80°N and 60°N (units: K). (e) Latitude-time evolution of zonal mean temperature anomalies at 10 hPa (shadings; units: K). (f) Pressure-time evolution of polar cap temperature anomalies (shadings; unit: K). (g) Pressure-time evolution of the standardized polar cap geopotential height anomalies (shadings).

short intermittent weakening of cold anomalies appeared during the first disturbance, and the warm anomalies reinforced during the minor and major SSWs.

The evolution of the standardized polar cap height anomalies that are a substitute for the NAM index was very similar to that of polar cap temperature anomalies (Fig. 2g), while the height anomalies extended from the stratosphere much lower to the troposphere than the temperature anomalies. The first stratospheric disturbance showed a simultaneous and lagged response in the troposphere, which is clearly shown by the positive height anomalies. During the minor SSW period, the stratospheric disturbance was not coupled to the troposphere. The tropospheric height anomalies lagged the stratospheric anomalies

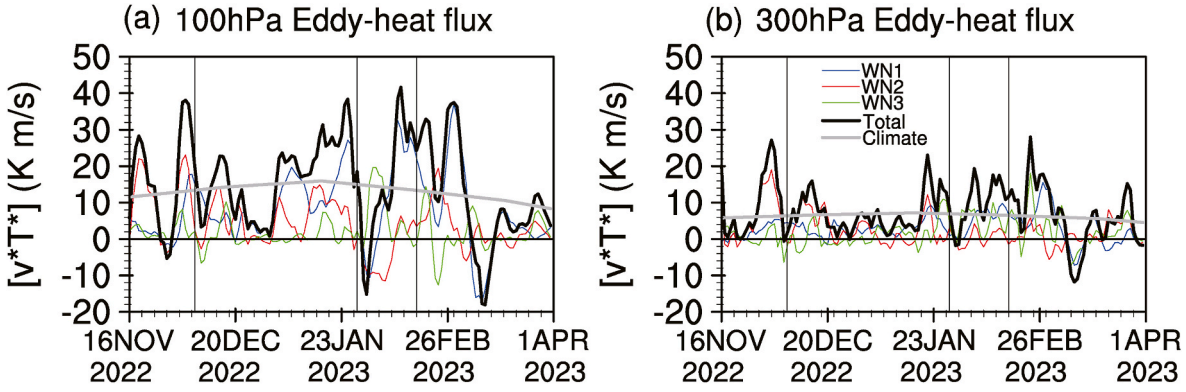

Fig. 3. Evolution of eddy heat flux by total waves (black), wavenumber 1 (blue), wavenumber 2 (red), and wavenumber 3 (green) averaged over the 45°N-75°N region (unit: K m/s) at (a) 100 hPa and (b) 300 hPa. The gray curve shows the climatological eddy heat flux by total waves. The vertical black line marks the onset date of stratospheric disturbance or the SSW.

during the third disturbance, suggesting a downward propagation of the stratospheric signals. By comparison, the response in the troposphere for the first disturbance and the major SSW was stronger than for the minor SSW.

The tropospheric planetary waves can propagate upward into the polar stratosphere and modulate the intensity of the stratospheric polar vortex. In order to attribute the contribution of planetary wavenumber 1 and wavenumber 2 in detail, Fig. 3 shows the mean eddy heat flux at 100 hPa and 300 hPa, respectively, which is proportional to the vertical component of the E-P flux. From 2 to 7 December, the total eddy heat flux was mainly contributed by the wavenumber 2 at both 100 and 300 hPa. Due to the short duration of the tropospheric wave pulse, the weak stratospheric polar vortex recovered very rapidly although it was elongated at 10 hPa in early winter. From 3 to 28 January, the total eddy heat flux at 100 hPa began to increase, exceeding its climatology. It was alternately contributed by the wavenumber 1 and wavenumber 2, but wavenumber 1 dominated and peaked before the onset date of the second stratospheric disturbance (i.e., the minor SSW with its onset on January 28). The eddy heat flux at 300 hPa also peaked on the onset date of the minor SSW, but it was equivalently contributed by wavenumbers 1, 2, and even 3. Since 9 February 2023, the total eddy heat flux contributed by wavenumber 1 increased rapidly at 100 hPa, inducing the occurrence of a major SSW on 16 February 2023. Since then, the wavenumbers 1 and 2 propagated upward alternately and persisted until 5 March 2023. Similarly, the total eddy heat flux dominated by the wavenumber 1 was also visible at 300 hPa, exceeding its climatology most of the time. It should be noted that the sudden increase in eddy heat flux at 300 hPa before December 7 and February 16 preceded that at 100 hPa, while on January 28 the wave pulse at 100 hPa was earlier than that at 300 hPa.

Fig. 4 shows the evolution of the stratospheric polar vortex in the Northern Hemisphere at 10 hPa during several peak periods of the eddy heat flux. From 2 to 7 December when the wavenumber 2 pulse dominated the total eddy heat flux, the polar vortex was elongated, with one of two centers extending toward Eurasia and the other toward North America. As a consequence, negative height anomalies were observed over the two northern continents, and an anomalous high center was observed in southern Greenland (Fig. 4a). From 13 to 18 January when the wavenumbers 1 and 2 contributed equally to the total eddy heat flux (Fig. 3a), the stratospheric polar vortex displaced toward Eurasia and North Atlantic, and the low height center was developed in an elliptical shape with the major axis extending from Greenland across the Arctic to Eurasia (Fig. 4b). The maximum low height anomalies can reach ~800 gpm. From 22 to 28 January when the total eddy heat flux was dominated by the wavenumber 1, the polar vortex shape did not show an evident change with the anomaly amplitude weakening (Fig. 4c). From 9 to 16 February when the total waves were dominated by the wavenumber 1, the polar vortex was displaced toward Eurasia with the positive height anomalies covering North America (Fig. 4d). From 17 to 22 February, the high pressure center over North Pacific moved to the Arctic when positive height anomalies covered the entire Arctic (Fig. 4e). From 25 February–3 March, the negative NAM pattern persisted (Fig. 4f).

The geopotential height anomalies at 500 hPa are shown in Fig. 5. From 2 to 7 December, the geopotential height anomalies show an obvious wavenumber 2 pattern, with the two low anomaly centers over East Asia and Canada, respectively and two high anomaly centers over North Pacific and North Atlantic, respectively. The anomalous wave 2 was in phase with the climatological wave 2 to increase the total planetary waves (Fig. 5a). The elongating of the stratospheric polar vortex was attributed to the upward propagation of waves. From 13 to 18 January 2023, the geopotential height anomalies presented a mixed wavenumbers 1 and 2 pattern. For example, the positive anomalies over the Urals and the negative anomalies over the coast of East Asia were in phase with the climatological wavenumber 2 pattern, which enhanced the climatological Ural high ridge and the East Asian trough (Fig. 5b). Similarly, the negative height anomalies over North Pacific and positive height anomalies over North Atlantic could increase the amplitude of the climatological wavenumber 1. From 22 to 28 January 2023, the positive height anomalies from Western Europe to the Atlantic coast and

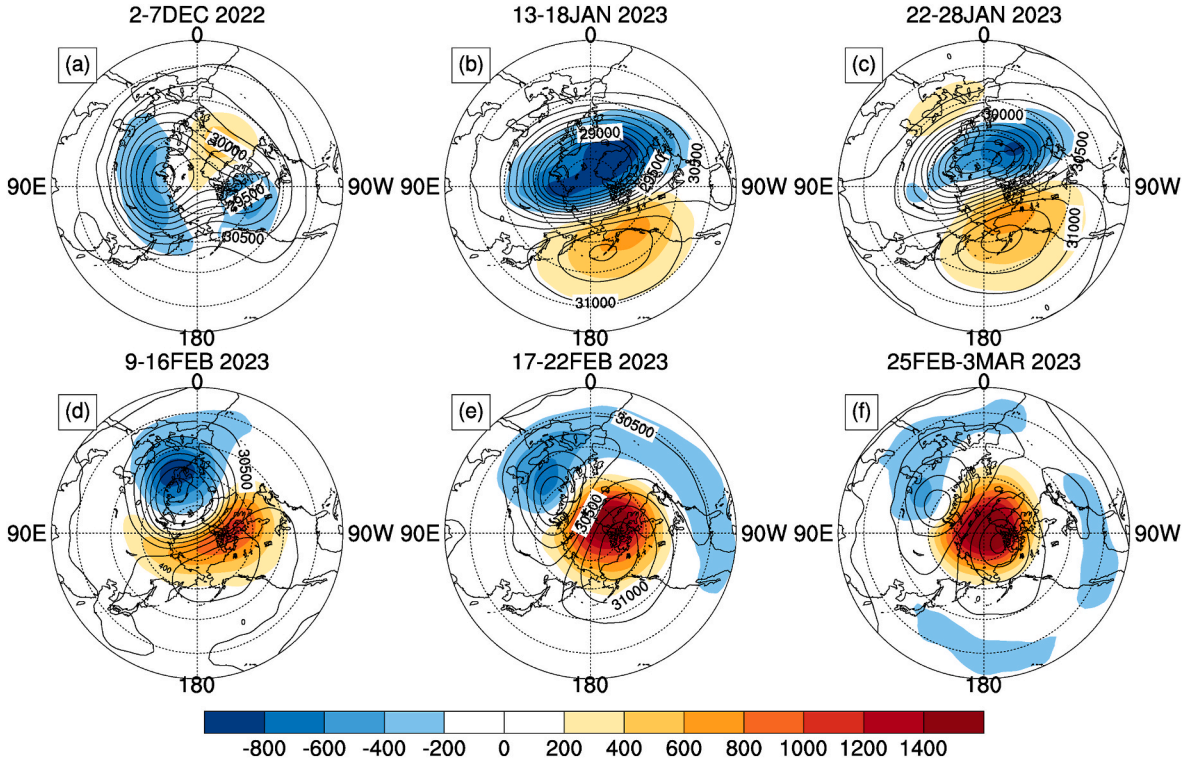

Fig. 4. Evolution of the polar vortex at 10 hPa (contour; unit: gpm) and the geopotential height anomalies (shadings; unit: gpm) in six periods.

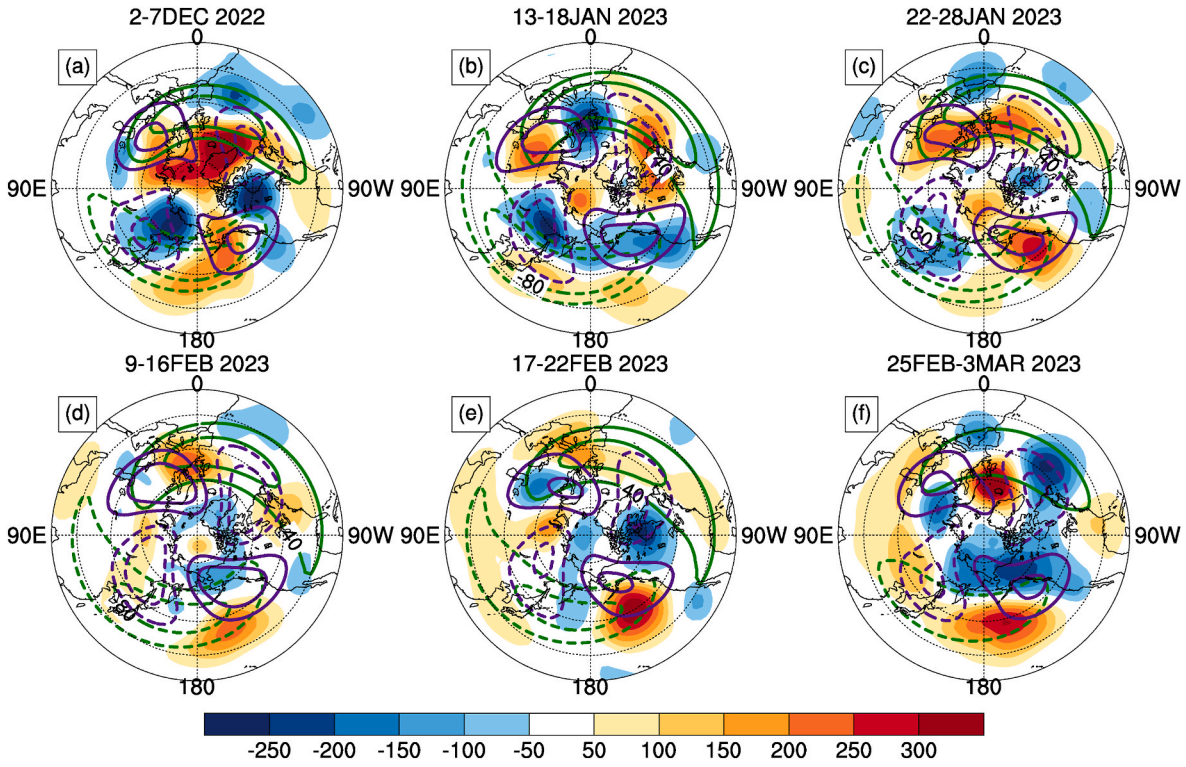

Fig. 5. Evolution of geopotential height anomalies at 500 hPa (shadings; unit: gpm) and distribution of the climatological wavenumber 1 and wavenumber 2 (contours; unit: gpm).

negative height anomalies over East Asian coasts resembled a wavenumber 1 pattern, which overlayed its climatology (Fig. 5c). Further, the negative height anomalies over East Asia and the positive height anomalies over the Eastern Pacific were in phase with the climatological wavenumber 2.

From 9 to 16 February 2023, the height anomalies began to decrease (Fig. 5d), consistent with the evolution of the eddy heat flux (Fig. 3). During 17–22 February, the height anomalies in the troposphere redeveloped: the positive anomaly center over the Northeast Pacific and the negative anomaly center over Arctic Canada were in phase with the climatological wavenumber 2, and the Pacific-North America pattern developed towards the negative phase, which denoted an increase of total waves (Fig. 5e). From 25 February–2 March, the downward propagation of stratospheric signals affected the troposphere with a negative NAO like pattern over the North Atlantic sector, and the height anomalies in the middle troposphere were out of phase with the climatological wavenumbers 1 or 2 (Fig. 5f).

4. Climate anomalies during the winter of 2022/23

4.1. Evolution of the stratospheric water vapor and ozone

The distribution of trace gases during the stratospheric disturbance can reflect the changes of the stratospheric circulation and help to reveal the dynamic mechanism in the stratosphere (Schoeberl and Hartmann, 1991; Manney et al., 2009). Fig. 6 shows the evolution of the distribution of water vapor and ozone, and the standardized vertical component of the BD circulation from 16 November 2022 to 1 April 2023 in the polar cap region. Fig. 6a shows the changes in stratospheric water vapor in the Arctic region, and it can be observed that high concentrations of water vapor in the stratosphere are mainly concentrated near the stratopause. During the strong polar vortex stage between the first stratospheric polar vortex disturbance and the minor SSW, the high concentration region of water vapor is located at 2–5 hPa, with a maximum water vapor content of 3.8 ppm. After the occurrence of minor SSW, the high concentration zone of water vapor rose to above 2 hPa, and after the major SSW onset, the highest water vapor content center exceeded 4 ppm. The eruption of the Tonga volcano on 15 January 2022 injected a large amount of sulfate and water vapor into the stratosphere, and it was estimated the water vapor increased in the stratosphere by ~10% (Millán et al., 2022). Under the effect of BD circulation, water vapor from tropical regions could be transported to the Arctic region. Fig. 6b shows that the water vapor in the middle and lower stratosphere below 50 hPa in the Arctic region is more than 6% higher. The negative anomalies of water vapor in the upper stratosphere gradually propagate downwards after the first polar vortex disturbance. After the major SSW onset, the water vapor is 3% less and the anomaly signal propagates downwards to 10 hPa. Fig. 6c shows the latitude-time evolution of water vapor at 10 hPa. It can be seen that the positive water vapor anomalies propagate from the tropics to the Arctic. After the major SSW onset, the positive water vapor anomalies only propagate northward to 60°N. From the standardized vertical residual velocity in the Arctic and tropical regions, it can be seen that before the three stratospheric disturbances there were some increase pulses in the upward airflow of the residual circulation in the tropical region and in the downward airflow in the polar region (Fig. 6g and h). The enhancement of the sinking branch of the BD circulation near the polar region explains the downward propagation of negative water vapor anomalies in the upper stratosphere from 20 December to 26 February, especially after the major SSW onset. However, the water vapor in the middle and lower stratosphere in polar regions increases.

Similar to the distribution of water vapor, ozone in the stratosphere is mainly concentrated in the upper stratosphere at 20-1 hPa. After the minor SSW onset on 28 January, the ozone concentration in the upper stratosphere increased to 9 ppm. After the major SSW on 16 February, the ozone concentration continued to rise, and ~10 ppm center appeared successively at 10 hPa and 2–5 hPa. With the strengthening of BD circulation during the three stratospheric disturbances (Fig. 6g and h), the ozone content in the middle stratosphere increased (Fig. 6d, e). Especially after the major SSW on 16 February, the ozone content in the

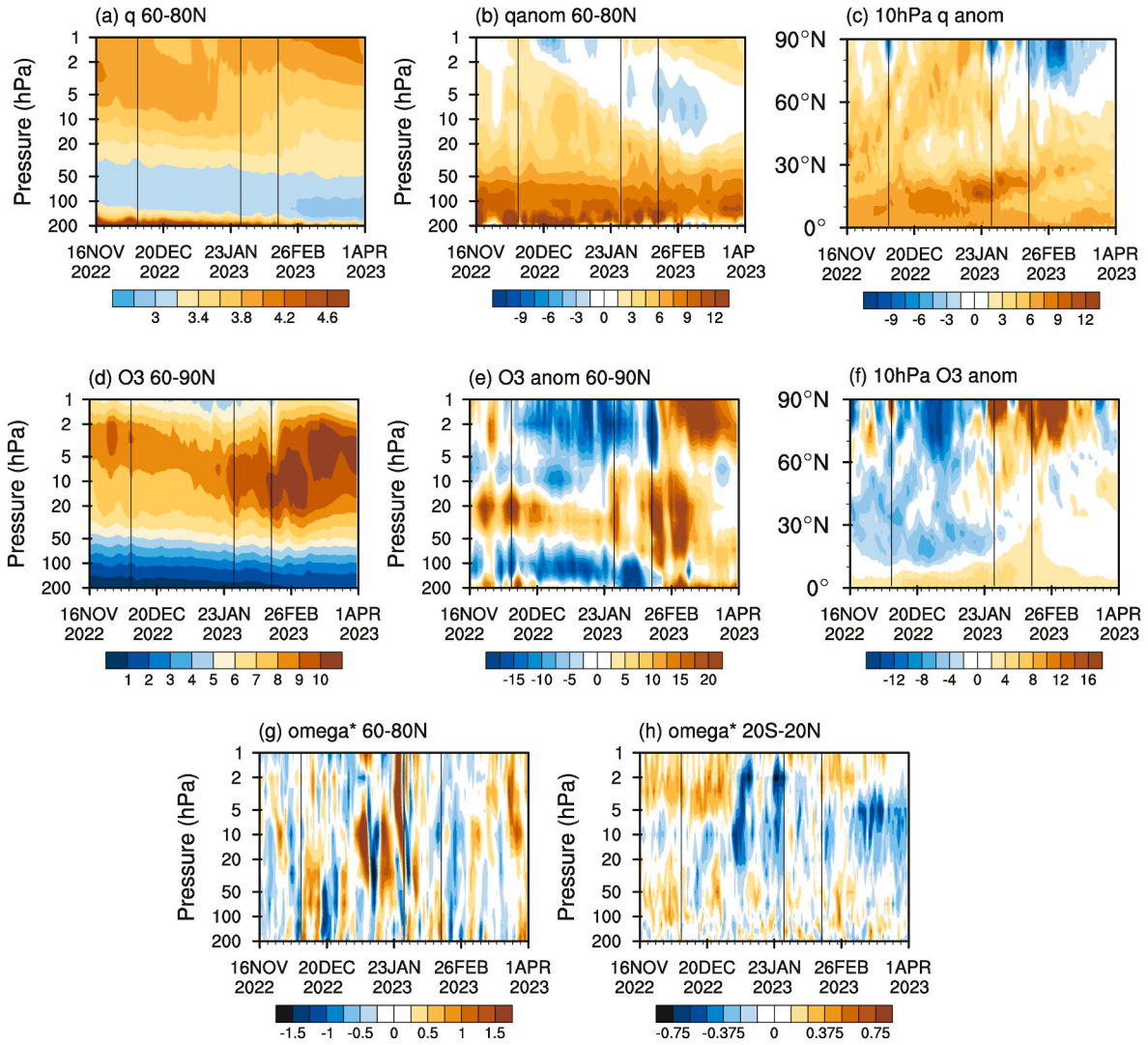

Fig. 6. Time evolutions of several metrics averaged over the polar cap region from 16 November 2022 to 1 April 2023. (a) Pressure-time evolution of water vapor (units: ppm). (b) Pressure-time evolution of the water vapor content anomalies relative to long-term climatology. (units: %). (c) Latitude-time evolution of the water vapor content anomalies relative to long-term climatology. (d) Pressure-time evolution of ozone (units: ppm). (e) Pressure-time evolution of the ozone content anomalies relative to long-term climatology (units: %). (f) Latitude-time evolution of the ozone content anomalies relative to long-term climatology (units: %). (g) Pressure-time evolution of the standardized vertical residual velocity in the Arctic region. (h) As in (e) but for the tropics.

middle and lower stratosphere was ~20% higher than the climatology. From the latitude-time evolution of ozone at 10 hPa, positive ozone anomalies are observed to propagate from the midlatitudes to the Arctic. The ozone content near the stratopause, which is close to 1 hPa, is ~20% higher than the climatology in half a month after the major SSW onset (Fig. 6e and f). It has been reported that SSWs lead to negative chemical tendencies for ozone during the initial warming of the SSW, and positive chemical tendencies as the vortex starts to recover at pressure levels above 20 hPa (de la Cámara et al., 2018b), which explains the increase in ozone content at the stratopause.

Fig. 7 shows the distribution of the stratospheric column ozone anomalies and height anomalies at 50 hPa in the polar region of the Northern Hemisphere for six focused periods. The geopotential height anomalies reflect the changes in polar vortex regimes, and the positive ozone anomalies basically correspond to the positive geopotential height anomalies after the major SSW onset. From 4 to 8 December 2022, ozone concentration was high in northeastern Asia, eastern North America, and the United Kingdom–western Europe (Fig. 7a). From 22 December 2022 to 13 January 2023, ozone concentration was low in the polar cap region and northern North America, and over northern Eurasia was relatively high (Fig. 7b). From 26 to 31 January, ozone concentration in eastern North America increased (Fig. 7c). From 4 to 9 February, ozone concentration in northeastern Eurasia–northeastern North America increased (Fig. 7d). As the stratospheric polar vortex was displaced from the Arctic after the major SSW, ozone concentrations in the polar cap region increased (Fig. 7e and f).

4.2. *Evolution of near-surface temperature*

Fig. 8 shows the distribution of 2-m temperature (t2m) anomalies in the winter of 2022/23. From 2 to 12 December 2022 (around the first stratospheric disturbance on 7 December 2022), the Eurasian continent was instantly covered with cold anomalies with a maximum anomaly amplitude >12 °C (Fig. 8a). This cold surge in midlatitude Eurasia was closely related to the strengthening of the Ural blocking and deepening of the East Asian trough, which together amplified the total planetary waves in the troposphere (Fig. 5a). Further, during the first stratospheric disturbance period, it showed a simultaneous and lagged response in the troposphere (Fig. 2). From 13 to 23 December 2022, about half a month after the occurrence of the first stratospheric disturbance, strong cold anomalies were observed in both East Asia and North America (Fig. 8b). This cold pattern over both continents was reminiscent of the cold

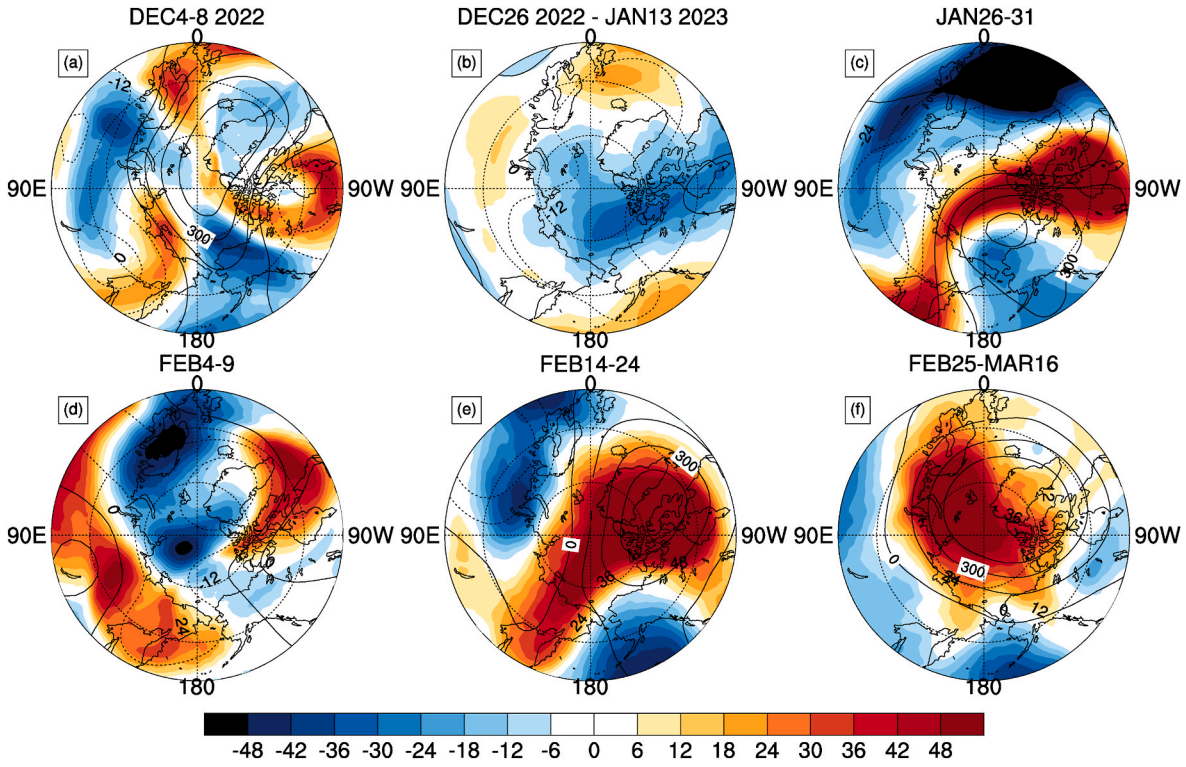

Fig. 7. Distribution of stratospheric column ozone anomalies (shadings; units: DU) and height anomalies at 50 hPa (contour; units: gpm).

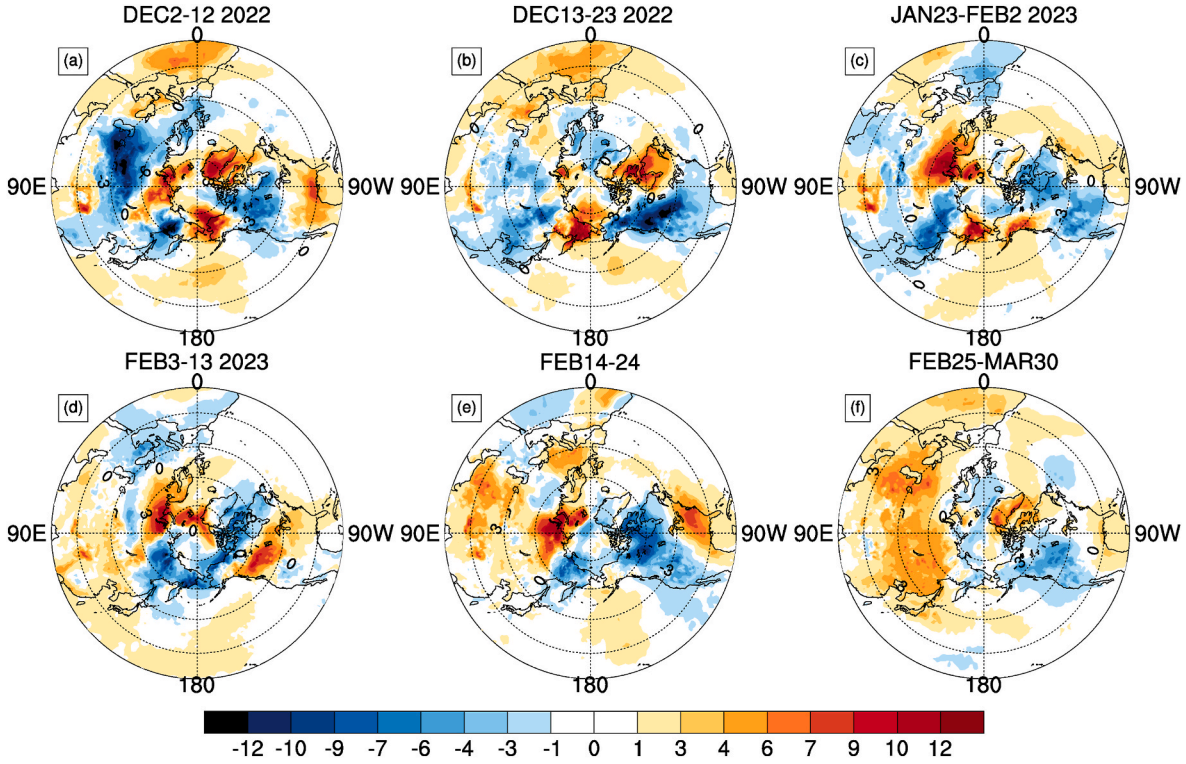

Fig. 8. Evolution of the 2-m temperature anomalies in the winter of 2022/23 in six focused periods (units: °C).

anomalies after the SSW onset in previous studies (Lu et al., 2021b; Rao et al., 2021). Recent studies have also confirmed that both SSW and SPV stretching are related to the cold temperature anomalies in North America (Cohen et al., 2021; Ding et al., 2023). During the second stratospheric disturbance from 23 January to 2 February 2023 (with the onset date of the minor SSW on 28 January 2023), cold anomalies were still present in both Eurasia and North America (Fig. 8c), with the coldness in East Asia further strengthening. From 3 to 13 February 2023 in 1–2 weeks following the second stratospheric disturbance, warm anomalies were observed in most of the Eurasian and North American

continents, with cold anomalies only observed in southern Europe (Fig. 8d). After the major SSW onset from 14 to 24 February 2023 (Fig. 8e), cold surge appeared in North America. Consistent with Lu et al. (2022a), cold anomalies are usually absent over the Eurasian continent following the displacement SSW. Cold anomalies over North America were persistent and still clearly presented during 25 February–30 March 2022.

5. Oceanic and atmospheric conditions during the winter of 2022/23

Previous studies have shown that certain Madden-Julian Oscillation (MJO) phases, the easterly phase of the QBO at 30 or 50 hPa, cold (La Niña) and warm (El Niño) phases of ENSO, and loss of Arctic sea ice are all conducive to the formation of the weakened stratospheric polar vortex (Baldwin et al., 2021; Garfinkel et al., 2012; Lu et al., 2021b; Rao et al., 2019a; Wheeler and Hendon, 2004).

From 5 to 15 February 2023, two weeks before the major SSW (16 February) onset, the MJO was in its phases 4–6 with the amplitude exceeding 1.5σ(Fig. 9d). Tropical convection in the western Pacific region is conducive to exciting the positive PNA response in the extratropics and enhancing the upward propagation of extratropical planetary waves, consistent with previous studies (Garfinkel et al., 2012; Wheeler and Hendon, 2004).

The Niño 3.4 index (5°S–5°N, 170°–120°W), normalized sea ice anomalies (detrended) in the Barents-Laptev (BL) Sea region

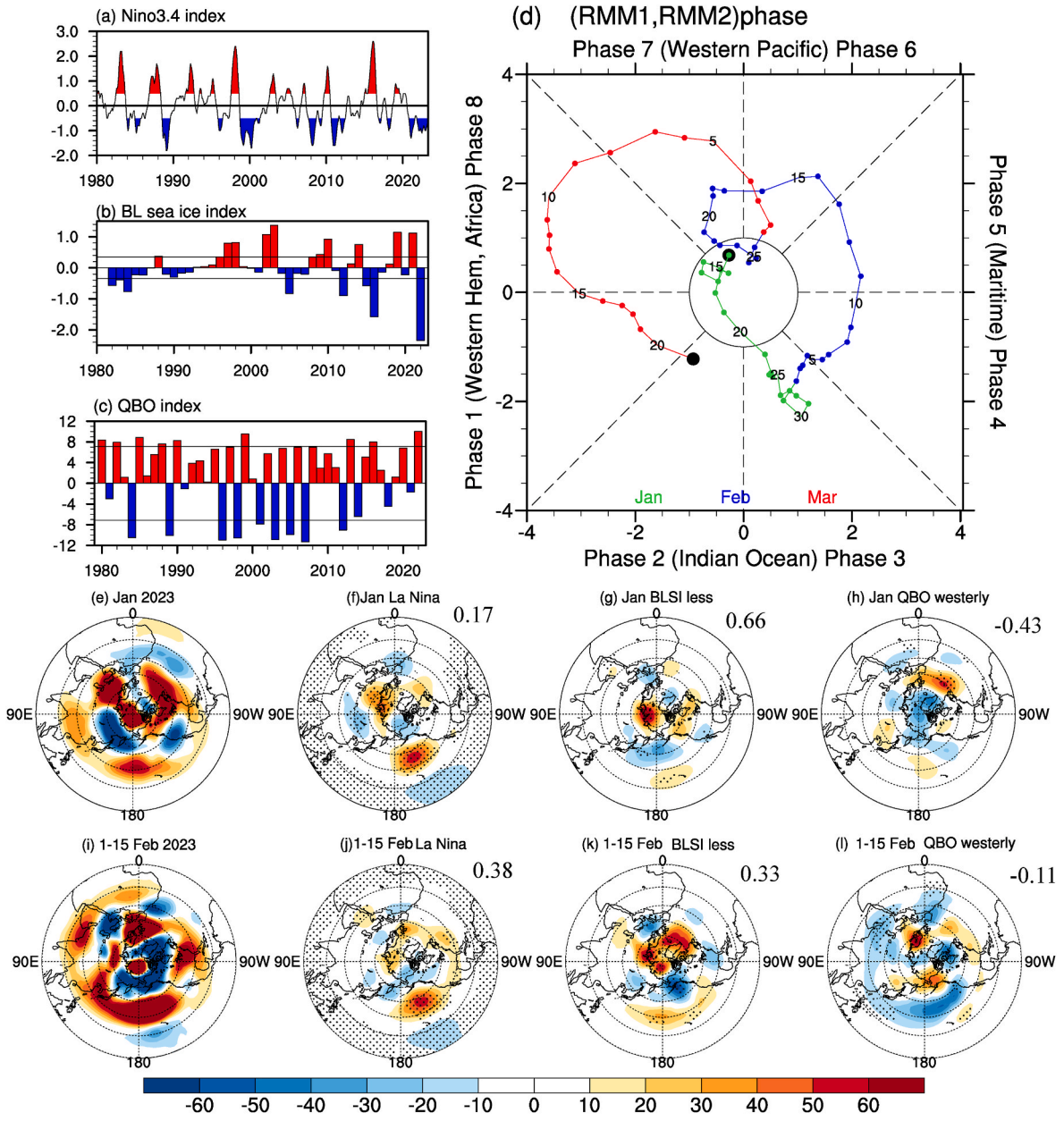

Fig. 9. (a) Time series of the Niño 3.4 index in December–January (unit: °C) from 1980 to 2023. The El Niño and La Niña states were shaded with red and blue colors. (b) Detrend normalized sea ice index in the Barents-Laptev Sea region (30°E–150°E, 72°E–83°N) averaged for December–January from 1980 to 2023 with the ±0.5σ marked by the horizontal reference lines. (c) QBO index (unit: m/s) at 50 hPa with the ±1.0σ marked by the horizontal reference lines. (d) Real-time multivariate MJO index from 10 January to 20 March 2023. (e) Geopotential height anomalies at 500 hPa in January 2023 (unit: gpm). (f) Composite geopotential height anomalies at 500 hPa in January for La Niñas. (g) Composite geopotential height anomalies at 500 hPa in January for Barents-Laptev Sea ice loss. (h) Composite geopotential height anomalies at 500 hPa in January for QBO westerlies. (i–l) As in (e–h) but for composite during 1–15 February. The black dots represent the composite height anomalies above the 95% confidence level using the Student *t*-test.

(30°–150°E, 72°–83°N) and QBO index (5°S–5°N) at 50 hPa averaged for December and January are shown in Fig. 9. The winter of 2022/23 can be found in the third year of a persistent La Niña state (Fig. 9a) with the Niño 3.4 index below −0.5 °C. The composite height anomalies at 500 hPa in January and the first half of February for La Niñas show that cold sea surface temperature anomalies in the tropical middle and east Pacific trigger an anomalous high center over the North Pacific in both January (pattern correlation or PCC = 0.17) and the first half of February (PCC = 0.38) (Fig. 9f, j vs Fig. 9e, i). The strong negative PNA response following the onset of the major SSW was mainly attributed to the La Niña forcing.

The detrended sea ice in the BL Sea region during December 2022–January 2023 was recorded as the lowest in the past 40 years (Fig. 9b). The composite height anomalies at 500 hPa for BL sea ice loss index ($<-0.5\sigma$) in January are highly correlated with the anomaly field in January 2023 (PCC = 0.66) (Fig. 9g). The BL sea ice loss induced the positive height anomalies in the Arctic and negative height anomalies in the Aleutian Islands in January (Fig. 9g). In the first half of February, the pattern correlation decreased to 0.33: The BL sea ice loss can induce negative height anomalies over Alaska and positive height anomalies over the North Pacific in the first half of February, explaining much less of the observed height anomaly pattern in the first half of February 2023 (PCC = 0.33, Fig. 9k vs Fig. 9i).

The QBO index is calculated using the averaged zonal wind anomaly from 5°S to 5°N at 50 hPa in winter (December–February). The QBO index in 2022/23 winter developed toward the westerly phase (Fig. 9c), which was unfavorable for the persistence of the weak stratospheric polar vortex (Holton and Tan, 1980; Rao et al., 2020a; 2023a). The composite height anomalies at 500 hPa in January were negatively correlated with the observed anomalies in January 2023 (PCC = −0.43, Fig. 9h), indicating that the QBO alone failed to explain the observed height anomalies in January 2023. Similar conditions are also applicable to the first half of February when the troposphere responds to the QBO in a positive NAM-like circulation pattern (PCC = −0.11, Fig. 9l). Therefore, the QBO was not responsible for the enhancement of the tropospheric waves in January and the first half of February 2023.

In summary, enhanced planetary wave activities sourced from the troposphere during the winter of 2020/23 were associated with the persistent La Niña and reduced BL sea ice. The major SSW occurred following phases 4–6 of the MJO. However, there are also other possible factors that are not considered here but may have played a role for the occurrence of major SSW.

6. Summary

Using the ERA5 reanalysis, sea surface temperature, sea ice observations, and real-time multivariate MJO index, the evolution of the stratospheric disturbances in the winter of 2022/23, the favorable conditions for their occurrence, and their possible effects on stratospheric ozone, water vapor, and near-surface temperature are explored. The main conclusions are as follows.

I. In the winter of 2022/23, three noticeable stratospheric disturbances were observed. The first disturbance was a weak polar vortex elongating in early winter, albeit with a short duration and only the zonal winds at 80°N reversed to easterlies. Although the abrupt increase in the polar temperature was not observed, the simultaneous and lagged responses of easterly anomalies and positive geopotential height anomalies were observed in the troposphere. The second stratospheric disturbance was a minor SSW with the polar vortex displaced toward Eurasia and North Atlantic on 28 January 2023 when a reversal of the polar temperature gradient was observed at 10 hPa. However, the minor SSW did not show a deep downward propagation into the troposphere. The third stratospheric disturbance was a displacement major SSW, which began on 16 February 2023 and continued until the end of March 2023, with the stratospheric signals propagating downward to the troposphere and near-surface.
II. Around 7 December 2022, a brief and intense wavenumber 2 pulse was observed in both the troposphere and stratosphere, although the duration was very short. This finally led to the elongating of the stratospheric polar vortex at 10 hPa during the first disturbance. In January 2023, the eddy heat flux was contributed alternately by planetary wavenumbers 1 and 2 (still dominated by the wavenumber 1 most of the time). Abundant eddy heat flux continued to accumulate in the stratosphere and resulted in the second disturbance, i.e., the minor SSW onset on 28 January 2023 with the polar vortex displaced towards Eurasia and North Atlantic. Since 9 February 2023, the total eddy heat flux by planetary wavenumber 1 increased rapidly, which corresponded to the third disturbance, i.e., the major SSW.
III. During the three polar stratospheric disturbances, the BD circulation showed three enhanced disturbances, characterized by both increased sinking motion in the Arctic and rising motion in the tropical regions, with the longest disturbance duration during the SSW period. Under the influence of the BD circulation, the water vapor and ozone in the middle and lower layers of the polar stratosphere show an increasing tendency, while the water vapor and ozone in the upper stratosphere show a decreasing tendency. However, after the major SSW onset, chemical reactions caused a rapid increase in ozone concentration in the upper stratosphere.
IV. During the first stratospheric disturbance on 7 December 2022, strong stratosphere-troposphere coupling occurred. During 2–12 December, the Ural ridge strengthened, and the East Asian trough deepened, which together amplified the planetary wavenumber 2. Continent cold surges occurred in Eurasia and North America. From 13 to 23 December 2022, there was still a strong response in the troposphere, and large cold anomalies occurred in North America. During the minor SSW period around 28 January, cold surges were weak, corresponding to the non-downward propagation of stratospheric disturbance. After the onset of the major SSW on 16 February, cold surges appeared in North America, although Eurasia was anomalously warm.
V. In the winter of 2022/23, the sea ice cover in the Barents-Laptev Sea area reached its lowest value since 1980. Further, the tropical Pacific sea surface temperature was anomalously cold in the third year of a long-lived La Niña state from autumn 2020–February 2023. Composite analysis revealed that the sea ice loss in the Barents-Laptev Sea and the La Niña partially explained the observed circulation anomalies in the winter of 2022/23. Two weeks before the onset of major SSW on 16 February, phases 4–6 of the MJO developed, which was conducive to the occurrence of the SSW. The westerly phase of QBO was not responsible for the frequent stratospheric disturbances in the winter of 2022/23.

It is worth noting that the short-lived stratospheric disturbance does not necessarily lead to a weak near-surface response. For example, although the first stratospheric disturbance around 7 December in the winter of 2022/23 only persisted for one week, the near-surface cold anomalies over both Eurasia and North America were even greater than the other two disturbances. Interactions between the stratosphere and troposphere might amplify the near-surface response to the stratosphere, and factors controlling the downward impact of stratospheric disturbances are also not clearly understood, and are left for future study.

Funds

This work was supported by the National Natural Science Foundation of China (42288101, 42322503, and 42175069), the 2023 Innovation Plan Project of Jiangsu Province (KYCX23_1 303), the Qinglan Project of

Jiangsu of China, and Chengde Basic Research Project (202205B065).

Author statement

Qian Lu (First Author): Data Curation, Software, Investigation, Formal Analysis, Writing - Original Draft; Jian Rao (Corresponding Author): Methodology, Formal Analysis, Writing - Original Draft; Chunhua Shi: Methodology, Formal Analysis, Writing - Review & Editing; Rongcai Ren: Methodology; Writing - Review & Editing; Yimin Liu: Funding Acquisition, Writing - Review & Editing; Siming Liu: Software, Investigation.

Declaration of competing interest

The authors declare that they have no known competing financial interests or personal relationships that could have appeared to influence the work reported in this paper.

Data availability

Data will be made available on request.

Acknowledgements

The work of data analysis and paper writing was conducted at Key Laboratory of Meteorological Disaster, Ministry of Education in Nanjing University of Information Science and Technology. The authors thank ECMWF (https://cds.climate.copernicus.eu) for their providing the ERA5 reanalysis data. The NECP/NCAR reanalysis is available from the NOAA Physical Sciences Laboratory (https://psl.noaa.gov/data/gridded/data.ncep.reanalysis.html). The monthly sea ice concentration and sea surface temperature from 1979 to 2020 are obtained from the Met Office Hadley Centre (https://www.metoffice.gov.uk/hadobs/hadisst/data/download.html). The real time multivariate Madden Julian Oscillation (MJO) index is available from the Australian Bureau of Meteorology (http://www.bom.gov.au/climate/mjo/graphics/rmm. 74toRealtime.txt).

References

Andrews, D.G., Holton, J.R., Leovy, C.B., 1987. Middle Atmosphere Dynamics. Academic Press, New York.
Allen, D.R., Coy, L., Eckermann, S.D., McCormack, J.P., Manney, G.L., Hogan, T.F., Kim, Y.J., 2006. NOGAPS-ALPHA simulations of the 2002 Southern Hemisphere stratospheric major warming. Mon. Weather Rev. 134, 498–518.
Andrews, M.B., Knight, J.R., Scaife, A.A., Lu, Y., Wu, T., Gray, L.J., Schenzinger, V., 2019. Observed and simulated teleconnections between the stratospheric quasi-biennial oscillation and northern Hemisphere winter atmospheric circulation. J. Geophys. Res. Atmos. 124, 1219–1232.
Anstey, J.A., Shepherd, T.G., 2014. High-latitude influence of the quasi-biennial oscillation. Q. J. R. Meteorol. Soc. 140, 1–21.
Baldwin, M.P., Ayarzagüena, B., Birner, T., Butchart, N., Butler, A.H., Charlton-Perez, A. J., Domeisen, D.I.V., Garfinkel, C.I., Garny, H., Gerber, E.P., Hegglin, M.I., Langematz, U., Pedatella, N.M., 2021. Sudden stratospheric warmings. Rev. Geophys. 59, e2020RG000708.
Baldwin, M.P., Dunkerton, T.J., 2001. Stratospheric harbingers of anomalous weather regimes. Science 294, 581–584.
Baldwin, M.P., Thompson, D.W.J., 2009. A critical comparison of stratosphere–troposphere coupling indices. Q. J. Roy. Meteorol. Soc. 135, 1661–1672.
Boljka, L., Birner, T., 2020. Tropopause-level planetary wave source and its role in two-way troposphere–stratosphere coupling. Weather Clim. Dyn. 1, 555–575.
Butler, A.H., Seidel, D.J., Hardiman, S.C., Butchart, N., Birner, T., Match, A., 2015. Defining sudden stratospheric warmings. Bull. Am. Meteorol. Soc. 96, 1913–1928.
Butler, A.H., Gerber, E.P., 2018. Optimizing the definition of a sudden stratospheric warming. J. Clim. 31, 2337–2344.
Cao, C., Chen, Y., Rao, J., Liu, S., Li, S., Ma, M., 2019. Statistical characteristics of major sudden stratospheric warming events in CESM1-WACCM : a comparison. Atmos 10, 1–18.
Charlton, A.J., Polvani, L.M., 2007. A new look at stratospheric sudden warmings. Part I: climatology and modeling benchmarks. J. Clim. 20, 449–469.
Charney, J.G., Drazin, P.G., 1961. Propagation of planetary-scale disturbances from the lower into the upper atmosphere. J. Geophys. Res. 66, 83–109.
Chen, W., Wei, K., 2009. Interannual variability of the winter stratospheric polar vortex in the Northern Hemisphere and their relations to QBO and ENSO. Adv. Atmos. Sci. 26, 855–863.
Cohen, J., Agel, L., Barlow, M., Garfinkel, C.I., White, I., 2021. Linking Arctic variability and change with extreme winter weather in the United States. Science (80 373, 1116–1121.
Dai, Y., Hitchcock, P., Mahowald, N.M., Domeisen, D.I.V., Hamilton, D.S., Li, L., Marticorena, B., Kanakidou, M., Mihalopoulos, N., Aboagye-Okyere, A., 2022. Stratospheric impacts on dust transport and air pollution in West Africa and the Eastern Mediterranean. Nat. Commun. 13, 1–10.
de la Cámara, A., Abalos, M., Hitchcock, P., 2018a. Changes in stratospheric transport and mixing during sudden stratospheric warmings. J. Geophys. Res. Atmos. 123, 3356–3373.
de la Cámara, A., Abalos, M., Hitchcock, P., Calvo, N., Garcia, R.R., 2018b. Response of Arctic ozone to sudden stratospheric warmings. Atmos. Chem. Phys. 18, 16499–16513.
de la Cámara, A., Birner, T., Albers, J.R., 2019. Are sudden stratospheric warmings preceded by anomalous tropospheric wave activity? J. Clim. 32, 7173–7189.
Ding, X., Chen, G., Zhang, P., Domeisen, D.I.V., Orbe, C., 2023. Extreme stratospheric wave activity as harbingers of cold events over North America. Commun. Earth Environ. 4, 187.
Domeisen, D.I.V., Butler, A.H., 2020. Stratospheric drivers of extreme events at the Earth's surface. Commun. Earth Environ. 1, 59.
Domeisen, D.I.V., Butler, A.H., Charlton-Perez, A.J., Ayarzagüena, B., Baldwin, M.P., Dunn-Sigouin, E., Furtado, J.C., Garfinkel, C.I., Hitchcock, P., Karpechko, A.Y., Kim, H., Knight, J., Lang, A.L., Lim, E.P., Marshall, A., Roff, G., Schwartz, C., Simpson, I.R., Son, S.W., Taguchi, M., 2020a. The role of the stratosphere in subseasonal to seasonal prediction: 1. predictability of the stratosphere. J. Geophys. Res. 125, e2019JD030920.
Domeisen, D.I.V., Butler, A.H., Charlton-Perez, A.J., Ayarzagüena, B., Baldwin, M.P., Dunn-Sigouin, E., Furtado, J.C., Garfinkel, C.I., Hitchcock, P., Karpechko, A.Y., Kim, H., Knight, J., Lang, A.L., Lim, E.P., Marshall, A., Roff, G., Schwartz, C., Simpson, I.R., Son, S.W., Taguchi, M., 2020b. The role of the stratosphere in subseasonal to seasonal prediction: 2. predictability arising from stratosphere-troposphere coupling. J. Geophys. Res., e2019jd030923
Garfinkel, C.I., Feldstein, S.B., Waugh, D.W., Yoo, C., Lee, S., 2012. Observed connection between stratospheric sudden warmings and the Madden-Julian Oscillation. Geophys. Res. Lett. 39, L18807.
Held, I.M., Ting, M., Wang, H.L., 2002. Northern winter stationary waves: theory and modeling. J. Climate 15, 2125–2144.
Hersbach, H., Bell, B., Berrisford, P., Hirahara, S., Horányi, A., Muñoz-Sabater, J., Nicolas, J., Peubey, C., Radu, R., Schepers, D., Simmons, A., Soci, C., Abdalla, S., Abellan, X., Balsamo, G., Bechtold, P., Biavati, G., Bidlot, J., Bonavita, M., De Chiara, G., Dahlgren, P., Dee, D., Diamantakis, M., Dragani, R., Flemming, J., Forbes, R., Fuentes, M., Geer, A., Haimberger, L., Healy, S., Hogan, R.J., Hólm, E., Janisková, M., Keeley, S., Laloyaux, P., Lopez, P., Lupu, C., Radnoti, G., de Rosnay, P., Rozum, I., Vamborg, F., Villaume, S., Thépaut, J.N., 2020. The ERA5 global reanalysis. Q. J. R. Meteorol. Soc. 146, 1999–2049.
Karpechko, A.Y., Charlton-Perez, A., Balmaseda, M., Tyrrell, N., Vitart, F., 2018. Predicting sudden stratospheric warming 2018 and its climate impacts with a multimodel ensemble. Geophys. Res. Lett. 45, 13538–13546.
Kim, B.M., Son, S.W., Min, S.K., Jeong, J.H., Kim, S.J., Zhang, X., Shim, T., Yoon, J.H., 2014. Weakening of the stratospheric polar vortex by Arctic sea-ice loss. Nat. Commun. 5, 4646.
Liang, Z., Rao, J., Guo, D., Lu, Q., 2022. Simulation and projection of the sudden stratospheric warming events in different scenarios by CESM2 - WACCM. Clim. Dynam. 59, 3741–3761.
Limpasuvan, V., Thompson, D.W.J., Hartmann, D.L., 2004. The life cycle of the Northern Hemisphere sudden stratospheric warmings. J. Clim. 17, 2584–2596.
Liu, H.L., Roble, R.G., 2005. Dynamical coupling of the stratosphere and mesosphere in the 2002 Southern Hemisphere major stratospheric sudden warming. Geophys. Res. Lett. 32, L13804.
Lu, Q., Rao, J., Guo, D., Yu, M., Yu, Y., 2021a. Downward propagation of sudden stratospheric warming signals and the local environment in the Beijing-Tianjin-Hebei region: a comparative study of the 2018 and 2019 winter cases. Atmos. Res. 254, 105514.
Lu, Q., Rao, J., Liang, Z., Guo, D., Luo, J., Liu, S., Wang, C., Wang, T., 2021b. The sudden stratospheric warming in January 2021. Environ. Res. Lett. 16, 084029.
Lu, Q., Rao, J., Shi, C., Guo, D., Fu, G., Wang, J., Liang, Z., 2022a. Possible influence of sudden stratospheric warmings on the atmospheric environment in the Beijing-Tianjin-Hebei region. Atmos. Chem. Phys. 22, 13087–13102.
Lu, Q., Rao, J., Shi, C., Guo, D., Wang, J., Liang, Z., Wang, T., 2022b. Observational subseasonal variability of the PM2.5 concentration in the beijing-tianjin-hebei area during the january 2021 sudden stratospheric warming. Adv. Atmos. Sci. 39, 1623–1636.
Manney, G.L., Schwartz, M.J., Krüger, K., Santee, M.L., Pawson, S., Lee, J.N., Daffer, W. H., Fuller, R.A., Livesey, N.J., 2009. Aura Microwave Limb Sounder observations of dynamics and transport during the record-breaking 2009 Arctic stratospheric major warming. Geophys. Res. Lett. 36, L12815.
Matsuno, T., 1971. A dynamical model of the stratospheric sudden warming. J. Atmos. Sci. 28, 1479–1494.
Maycock, A.C., Hitchcock, P., 2015. Do split and displacement sudden stratospheric warmings have different annular mode signatures? Geophys. Res. Lett. 42, 10943–10951.
Millán, L., Santee, M.L., Lambert, A., Livesey, N.J., Werner, F., Schwartz, M.J., Pumphrey, H.C., Manney, G.L., Wang, Y., Su, H., Wu, L., Read, W.G., Froidevaux, L.,

2022. The hunga Tonga-hunga ha'apai hydration of the stratosphere. Geophys. Res. Lett. 49, e2022GL099381.
Nishii, K., Nakamura, H., Miyasaka, T., 2009. Modulations in the planetary wave field induced by upward-propagating Rossby wave packets prior to stratospheric sudden warming events: a case-study. Q. J. R. Meteorol. Soc. 135, 39–52.
Polvani, L.M., Waugh, D.W., 2004. Upward wave activity flux as a precursor to extreme stratospheric events and subsequent anomalous surface weather regimes. J. Clim. 17, 3548–3554.
Rao, J., Garfinkel, C.I., Chen, H., White, I.P., 2019a. The 2019 new year stratospheric sudden warming and its real-time predictions in multiple S2S models. J. Geophys. Res. Atmos. 124, 11155–11174.
Rao, J., Garfinkel, C.I., White, I.P., 2020a. Predicting the downward and surface influence of the February 2018 and january 2019 sudden stratospheric warming events in subseasonal to seasonal (S2S) models. J. Geophys. Res. Atmos. 125, e2019JD031919.
Rao, J., Garfinkel, C.I., White, I.P., Schwartz, C., 2020b. The southern Hemisphere minor sudden stratospheric warming in September 2019 and its predictions in S2S models. J. Geophys. Res. Atmos. 125, e2020JD032723.
Rao, J., Garfinkel, C.I., 2020a. CMIP5/6 models project little change in the statistical characteristics of sudden stratospheric warmings in the 21st century. Environ. Res. Lett. 16, 034024.
Rao, J., Garfinkel, C.I., 2020b. Arctic ozone loss in March 2020 and its seasonal prediction in CFSv2: a comparative study with the 1997 and 2011 cases. J. Geophys. Res. Atmos. 125, e2020JD033524.
Rao, J., Liu, S., Chen, Y., 2021. Northern Hemisphere sudden stratospheric warming and its downward impact in four Chinese CMIP6 models. Adv. Atmos. Sci. 38, 187–202.
Rao, J., Ren, R., Chen, H., Liu, X., Yu, Y., Yang, Y., 2019b. Sub-seasonal to seasonal hindcasts of stratospheric SuddenWarming by BCC_CSM1.1(m): a comparison with ECMWF. Adv. Atmos. Sci. 36, 479–494.
Rao, J., Garfinkel, C.I., Wu, T., Luo, J.J., Lu, Y., Chu, M., Lu, Q., 2023. Combined modes of the northern stratosphere, tropical oceans, and east Asian spring rainfall: a novel method to improve seasonal forecasts of precipitation. Geophys. Res. Lett. 50, e2022GL101360.
Rao, J., Wu, T., Garfinkel, C.I., Luo, J., Lu, Y., Chu, M., Hu, J., 2022. Impact of the initial stratospheric polar vortex state on East Asian spring rainfall prediction in seasonal forecast models. Clim. Dynam. 60, 4111–4131.
Rayner, N.A., Parker, D.E., Horton, E.B., Folland, C.K., Alexander, L.V., Rowell, D.P., Kent, E.C., Kaplan, A., 2003. Global analyses of sea surface temperature, sea ice, and night marine air temperature since the late nineteenth century. J. Geophys. Res. Atmos. 108 https://doi.org/10.1029/2002jd002670.
Schoeberl, M.R., Hartmann, D.L., 1991. The dynamics of the stratospheric polar vortex and its relation to springtime ozone depletions. Science 251, 46–52.
Seviour, W.J.M., Mitchell, D.M., Gray, L.J., 2013. A practical method to identify displaced and split stratospheric polar vortex events. Geophys. Res. Lett. 40, 5268–5273.
Shen, X., Wang, L., Osprey, S., 2020. The Southern Hemisphere sudden stratospheric warming of September 2019. Sci. Bull. 65, 1800–1802.
Thompson, D.W.J., Baldwin, M.P., Wallace, J.M., 2002. Stratospheric connection to Northern Hemisphere wintertime weather: implications for prediction. J. Clim. 15, 1421–1428.
Tian, W., Huang, J., Zhang, J., 2023. Role of stratospheric processes in climate change: advances and challenges. Adv. Atmos. Sci. 40, 1379–1400.
Tripathi, O.P., Baldwin, M., Charlton-perez, A., Charron, M., Stephen, D., Gerber, E., Harrison, R.G., Jackson, D.R., Kim, B., Kuroda, Y., Lang, A., Mahmood, S., Mizuta, R., Roff, G., Son, S., 2015. The predictability of the extratropical stratosphere on monthly time-scales and its impact on the skill of tropospheric forecasts. Q. J. R. Meteorol. Soc. 141, 987–1003.
Wheeler, M.C., Hendon, H.H., 2004. An all-season real-time multivariate MJO index: development of an index for monitoring and prediction. Mon. Weather Rev. 132, 1917–1932.
White, I., Garfinkel, C.I., Gerber, E.P., Jucker, M., Aquila, V., Oman, L.D., 2019. The downward influence of sudden stratospheric warmings: association with tropospheric precursors. J. Clim. 32, 85–108.
Yoden, S., Yamaga, T., Pawson, S., Langematz, U., 1999. A composite analysis of the stratospheric sudden warmings simulated in a perpetual january integration of the Berlin TSM GCM. J. Meteorol. Soc. Japan 77, 431–445.
Yu, Y., Ren, R., Cai, M., 2015. Dynamic linkage between cold air outbreaks and intensity variations of the meridional mass circulation. J. Atmos. Sci. 72, 3214–3232.
Zhang, J., Tian, W., Chipperfield, M.P., Xie, F., Huang, J., 2016. Persistent shift of the Arctic polar vortex towards the Eurasian continent in recent decades. Nat. Clim. Change 6, 1094–1099.